# Nuclear Spin Relaxation of Longitudinal and Singlet Order in Liquid-CO2 Solutions

Aliki Moysiadi[1], Francesco Giustiniano[1], Andrew M. Hall[1], Topaz A. Cartlidge[1], Lynda J. Brown[1], Giuseppe Pileio[1*]

[1]University of Southampton, United Kingdom

*Submitted to Journal:*
Frontiers in Chemistry

*Specialty Section:*
Physical Chemistry and Chemical Physics

*Article type:*
Original Research Article

*Manuscript ID:*
668044

*Received on:*
15 Feb 2021

*Revised on:*
23 Mar 2021

*Journal website link:*
www.frontiersin.org

## Conflict of interest statement

The authors declare that the research was conducted in the absence of any commercial or financial relationships that could be construed as a potential conflict of interest

## Author contribution statement

AM, FG and AMRH have equally contributed to this paper. AM and TAAC ran experiments and processed data; FG built the CO2 equipment and provided engineering support; AMRH built the sample shuttle, run experiments and processed data; LJB synthesised the molecules and provided chemical support. GP devised the research, ran some experiments and wrote the paper.


## Keywords

Singlet Spin Order, liquid-CO2, Nuclear Magnetic Resonance, Long-lived spin states, Nuclear spin relaxation



## Abstract

Word count: 129

Hyperpolarization techniques can enormously enhance the NMR signal thus allowing the exploitation of hyperpolarized substrates for in-vivo MRI applications. The short lifetime of hyperpolarized spin order poses significant limitations in such applications. Spin order storage can be prolonged through the use of long-lived spin states. Additionally, the storage of spin polarization - either in the form of longitudinal or singlet order - can be prolonged in low viscosity solutions. Here, we report the use of low viscosity liquid-CO2 solutions to store nuclear spin polarization in the form of longitudinal and singlet order and for extended periods. Our results demonstrate that this storage time can be considerably sustained in liquid-CO2 solutions in comparison to other low viscosity solvents, opening up the possibility of new, exciting storage experiments in the future.


## Contribution to the field

In this paper we have investigated the possibility to use liquid-CO2 as a solvent to store longitudinal and long-lived nuclear spin order for prolonged periods of time. The interest in doing such investigations lies with the fact that liquefied gases have quite low viscosities and this may, in selected circumstances as evidenced in this paper, prolong the storage time of nuclear polarisation. Moreover, liquid-CO2 can be easily removed by venting and replaced by other solvents rapidly; i.e. the conditions for the long term storage of polarisation can easily differ from the condition of use of the stored material. Our intention, and indeed the relevance of this paper, is to use liquid-CO2 to store hyperpolarised spin order so to allow transport to a remote location and/or facilitate any intermediate operation required in the interval between production of hyperpolarized order and its use. We believe this can facilitate applications of long-lived spin order in in-vivo MRI and molecular imaging.

## Ethics statements

### Studies involving animal subjects

Generated Statement: No animal studies are presented in this manuscript.

### Studies involving human subjects

Generated Statement: No human studies are presented in this manuscript.

### Inclusion of identifiable human data

Generated Statement: No potentially identifiable human images or data is presented in this study.

## Data availability statement

Generated Statement: The original contributions presented in the study are included in the article/supplementary material, further inquiries can be directed to the corresponding author/s.

# Nuclear Spin Relaxation of Longitudinal and Singlet Order in Liquid-$CO_2$ Solutions

**Aliki Moysiadi[1], Francesco Giustiniano[1], Andrew M. R. Hall[1], Topaz A. A. Cartlidge[1], L. J. Brown[1] and G. Pileio[1,*]**

[1] School of Chemistry, University of Southampton, SO17 1BJ, Southampton, UK

*** Correspondence:**
Corresponding Author
g.pileio@soton.ac.uk

**Keywords: Nuclear Spin Relaxation, Singlet Spin Order, Long-lived Spin States, liquid-$CO_2$**

## Abstract

Hyperpolarization techniques can enormously enhance the NMR signal thus allowing the exploitation of hyperpolarized substrates for *in-vivo* MRI applications. The short lifetime of hyperpolarized spin order poses significant limitations in such applications. Spin order storage can be prolonged through the use of long-lived spin states. Additionally, the storage of spin polarization - either in the form of longitudinal or singlet order - can be prolonged in low viscosity solutions. Here, we report the use of low viscosity liquid-$CO_2$ solutions to store nuclear spin polarization in the form of longitudinal and singlet order and for extended periods. Our results demonstrate that this storage time can be considerably sustained in liquid-$CO_2$ solutions in comparison to other low viscosity solvents, opening up the possibility of new, exciting storage experiments in the future.

## 1 Introduction

Molecules that contain an "isolated" spin-1/2 pair of nuclei, offer the possibility to prepare a form of spin order, namely, singlet spin order[1-3] with the fundamental property of being long-lived. This is due to the fact that singlet spin order decays at a much slower rate than the longitudinal spin order conventionally used in most NMR experiments. This form of order has already been used in a range of different applications including: high-sensitivity quantification of ligand binding[4, 5]; measurements of slow translational dynamics[6-11] and long-lived molecular tags to preserve information over a long time[12-22]. There is great potential for exploitation of long-lived spin order in high impact applications and in combination with techniques such as PHIP[23], SABRE[24] and dissolution-DNP[25] as a vehicle to preserve spin hyperpolarization. In the important fields of *in-vivo* MRI and molecular imaging, it is crucial to achieve the signal enhancement provided by such techniques. The capacity to preserve such enhancement for very long time periods so to allow quality controls, transport and injection into the patient offers an exciting step forward. Moreover, the possibility to preserve hyperpolarization for hour-long periods would allow delocalisation of the point-of-production (the hyperpolarization equipment) from the point-of-use (the NMR/MRI machine). This presents many advantages but perhaps the most important is that the point-of-use does not necessarily need to be equipped with hyperpolariser instrumentation and have specially trained personnel (in the case of dissolution-DNP this is very costly).

Recent progress in this field exploits the use, at the hyperpolarisation stage, of radical-containing porous matrices that would allow the storage of hyperpolarised longitudinal order in the form of a frozen solid which also displays very long lifetime[26].

Another possible way to achieve this decentralization involves the exploitation of long-lived spin states. Indeed, long-lived spin order with record lifetimes of 70 minutes in degassed acetone-$d_6$ solutions at 20 ºC and 0.4 T field[27] and of 108 minutes at 30 ºC and 0.25 T field[28] have been

reported. However, in general, the conditions which maximize the lifetime may be different to the conditions required at usage. For example, storage in a low-viscosity solvent such as acetone can prolong the lifetime of those states, but such solvent is clearly incompatible for use in a clinical setting.

The rationale behind why the lifetime of spin order can be prolonged in low-viscosity media arises from the very core of nuclear spin relaxation theory[29]. Spin relaxation is due to fluctuating magnetic field present in solutions. These fields have a different nature and are ultimately due to spin-spin, spin-field and spin-rotation interactions. The contributions from different mechanisms are additive to the total relaxation rate. Moreover, the spin-spin mechanism due to dipole-dipole interactions between the two spins in the spin-1/2 pair (ipDD) dominates the relaxation rate in the case of longitudinal spin order in degassed samples. The ipDD mechanism, however, does not affect the singlet order lifetime[30]. The spin-field mechanism due to the chemical shift tensor anisotropy (CSA) is, typically, the second in order of importance and affects both longitudinal and singlet order. Spin-rotation mechanisms due either to the coupling between spin and angular moment (SR) or to the coupling between spin and internal motions (SIM) are the next in terms of importance; all other mechanisms including dipole-dipole interaction with out-of-pair spins, interactions with spins in solvent molecules and so on are of minor importance and can be neglected in a first approximation. A detailed discussion of these mechanisms and their role in singlet order relaxation has been summarized in a book chapter[1].

The very fact that those magnetic fields fluctuate is due to the dynamics of molecules in solution including rotation, diffusion and collision events. The fundamental parameter used to characterize these fluctuations is the correlation time. The contribution to the total decay rate from ipDD and CSA mechanisms is proportional to a correlation time which is linked to the molecular rotational diffusion. This correlation time is usually indicated as $\tau_c$ but differentiated into $\tau_1$ and $\tau_2$ depending on the rank of the interaction (ipDD is a rank-2 interaction while CSA has rank-1 ($CSA^-$) and rank-2 ($CSA^+$) components). Both $\tau_1$ and $\tau_2$ are directly proportional to viscosity. Conversely, the contribution to the total decay rate from spin-rotation mechanisms is directly proportional to a correlation time which is linked to molecular collision. This correlation time is usually indicated as $\tau_{SR}$ but is inversely proportional to viscosity. This means that, depending on the relative strength of the active interactions, the longitudinal and singlet order lifetimes can be extended by reducing the viscosity of the solution. More appropriately, this lifetime extension is observed whenever the decay rates are dominated by mechanisms such as ipDD or CSA whereas the opposite could be observed when SR mechanisms prevails.

As a consequence, we were interested in exploring the use of liquified $CO_2$ gas as a low-viscosity solvent in which spin order can be stored either as longitudinal or singlet order. Pure liquid-$CO_2$ has a viscosity of 0.06 cP which is significantly lower than, for example, pure acetone-$d_6$ which has a viscosity of 0.34 cP, a factor of ~5.6 times lower. As previously outlined, in situations where ipDD and CSA relaxation mechanisms dominate, an elongation of singlet order lifetime is theoretically possible. A further significant advantage of exploiting liquid-$CO_2$ is the ability to rapidly evaporate this solvent by simply venting the NMR tube, thus allowing easy exchange with another solvent. This would facilitate experiments that employ one set of conditions to prolong the storage of hyperpolarization and other conditions for the time of use.

The use of $CO_2$ as a solvent in NMR is not new[31-36] but our contribution is the first report in which the properties of this solvent are investigated in the context of enhancing the lifetime of long-lived spin order.

Herein, we describe equipment built to prepare and handle NMR tubes filled with liquid-$CO_2$ solutions. We present a thorough investigation of the lifetime of longitudinal and singlet spin order in liquid-$CO_2$ solutions as compared with the same values measured in more conventional organic solvents. We report data measured at a wide variety of magnetic fields from 16.4 T to 50 mT for three different molecular systems that all support long-lived spin order. These findings are

discussed in terms of a simplified relaxation analysis, based on previously derived analytical equations, and we propose future experiments made possible by our results.

## 2 Materials and Methods

### 2.1 Instrumentation

Experiments presented in this paper were run on a variety of NMR instruments. Data at 16.4 T was collected on a Bruker 700 MHz Avance Neo spectrometer equipped with a 5mm TCI prodigy cryoprobe. Data at 11.7 T was collected on a Bruker 500 MHz Avance III spectrometer equipped with a 5mm TBO z-grad probe. Data at 7 T was collected on a Bruker 300 MHz Avance III spectrometer equipped with a Bruker MICWB40 microimaging probe carrying a $^{1}H/^{13}C$ 10 mm resonator. Data collected at magnetic fields below 7 T was collected in field-cycling mode by using an automatic sample shuttle[28] installed on the 300 MHz spectrometer.

### 2.2 Molecular systems

Experiments have been carried out on a variety of molecular systems which support long-lived spin states. The molecular structures of all systems employed are reported in Figure 1. The first molecule is a doubly-$^{13}C$-labelled and perdeuterated derivative of naphthalene, 1,2,3,4,5,6,8-heptakis(methoxy-$d_3$)-7-((propan-2-yl-$d_7$)oxy)-4a,8a-$^{13}C_2$-naphthalene (**Nap**). The second molecule is a doubly-$^{13}C$-labelled and perdeuterated unsymmetrical diester of acetylene dicarboxylic acid, 1-(methyl-$d_3$) 4-(propan-2-yl-$d_7$) but-2-ynedioate (**Act**). The third molecule is a perdeuterated unsymmetrical diester of the maleic acid, 1-(ethyl-$d_5$)-4-(propyl-$d_7$)(*Z*)-but-2-enedioate (**Mal**). All molecules have been synthesised in-house according to published procedures[37-39].

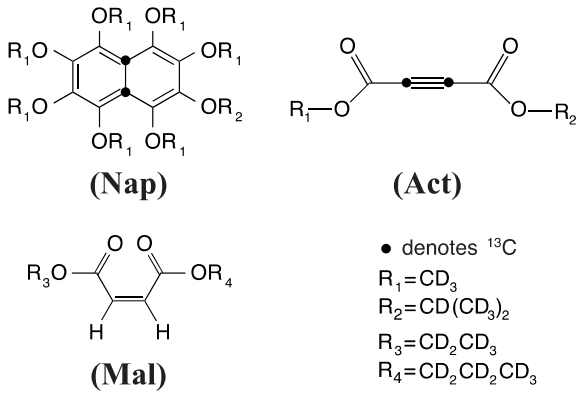


*Figure 1. Structure of the molecular systems employed in this work*

### 2.3 Samples

Molecules **Nap, Act** and **Mal** have been used to prepare several different samples. For clarity we have labelled all preparations with different names and these are summarized in Table 1. The sample nomenclature works as follow: the first three digits reflect the molecular system; the next three digits refer to the solvent in which the molecule has been dissolved; the last digit, when present, distinguishes similar samples prepared at different concentration as detailed in Table 1.

Samples were degassed to remove paramagnetic dissolved oxygen. Excluding liquid-$CO_2$ samples, degassing was done by ten freeze-pump-thaw cycles; the degassing procedure used for samples in liquid-$CO_2$ is described below.

*Table 1. Nomenclature and preparation details of all samples used in the paper*

| Sample Name | Molecular System | Solvent | Viscosity of pure solvent at 20 °C (cP)* | Concentration (mM) |
|---|---|---|---|---|
| **NapCo2a** | **Nap** | liquid-$CO_2$ (**Co2**) | 0.06 | 36 |
| **NapCo2b** | **Nap** | liquid-$CO_2$ (**Co2**) | 0.06 | 61 |
| **NapCo2c** | **Nap** | liquid-$CO_2$ (**Co2**) | 0.06 | 85 |
| **NapCo2d** | **Nap** | liquid-$CO_2$ (**Co2**) | 0.06 | 108 |
| **NapTbu** | **Nap** | t-butanol-$d_{10}$ (**Tbu**) | 4.3 | 200 |
| **NapDms** | **Nap** | DMSO-$d_6$ (**Dms**) | 2.4 | 200 |
| **NapEth** | **Nap** | Ethanol-$d_6$ (**Eth**) | 1.2 | 150 |
| **NapClf** | **Nap** | Chloroform-d (**Clf**) | 0.57 | 260 |
| **NapMet** | **Nap** | Methanol-$d_4$ (**Met**) | 0.52 | 160 |
| **NapAce** | **Nap** | Acetone-$d_6$ (**Ace**) | 0.34 | 200 |
| **NapCo2e** | **Nap** | liquid-$CO_2$ (**Co2**) | 0.06 | 50 |
| **ActClf** | **Act** | Chloroform-d (**Clf**) | 0.57 | 700 |
| **ActCo2** | **Act** | liquid-$CO_2$ (**Co2**) | 0.06 | 100 |
| **MalEth** | **Mal** | Ethanol-$d_6$ (**Eth**) | 1.2 | 500 |
| **MalCo2** | **Mal** | liquid-$CO_2$ (**Co2**) | 0.06 | 340 |

***** Handbuch der Instrumentellen Analytik NMR-spektroskopie provided by S. Thomas in "Spectroscopic Tools" URL: http://www.science-and-fun.de/tools/

## 2.4 High pressure tubes and volume restriction inserts

All samples other than those in liquid-$CO_2$ have been prepared in standard 5 or 10 mm LPV NMR tubes. Samples involving liquid-$CO_2$ are prepared in special high-pressure NMR tubes (purchased from Rototec-Spintec, DE) consisting of either a zirconia or sapphire tube connected to an aluminum needle-valve. High pressure tubes (5 mm) made of zirconia can withstand pressures up to 1000 bar whilst 10 mm high pressure tubes are made of sapphire and can withstand pressures up to 300 bar. To confine the sample within the coil region (so to minimize the effects of thermal convection) we constructed a glass insert consisting of two precision-manufactured filled glass rods and a piece of glass tube that fits inside the high-pressure tubes to confine the sample within a 10.5 mm cylindrical chamber placed in the middle of our 18 mm long coil. The insert outer diameter is slightly smaller than the high-pressure tube internal diameter (ID) leaving just a 250 $\mu$m gap. Tube construction and all dimensions are illustrated in Figure 2.

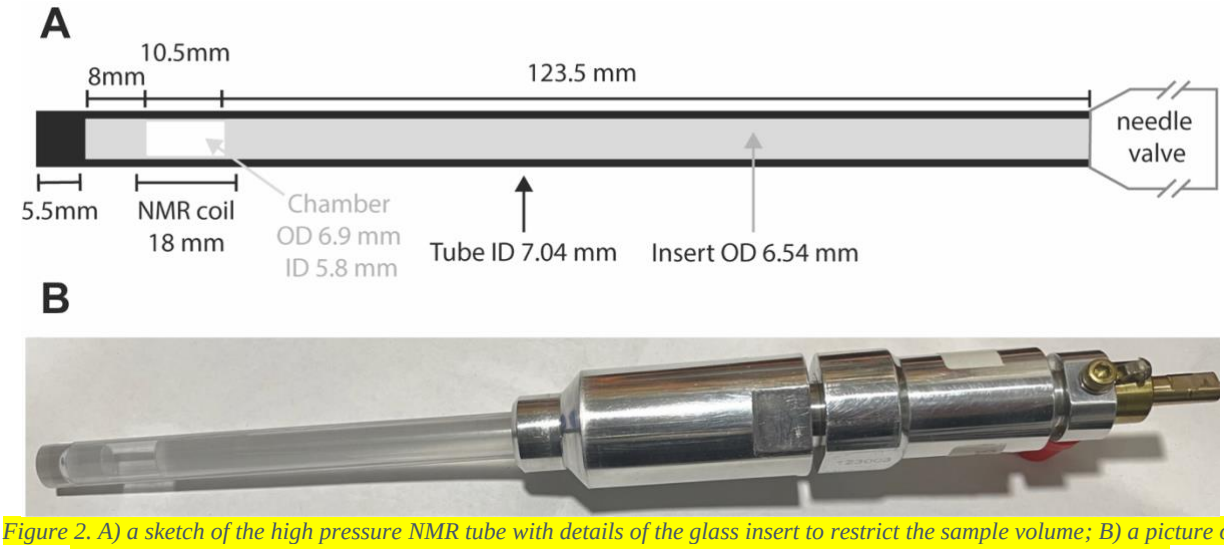


*Figure 2. A) a sketch of the high pressure NMR tube with details of the glass insert to restrict the sample volume; B) a picture of the actual 10 mm sapphire high pressure tube with the glass insert and filled with a solution of **Nap** in liquid-$CO_2$.*

## 2.5 $CO_2$ samples preparation

To allow preparation of samples in liquid-$CO_2$ specialist equipment was required. The apparatus was constructed as diagrammatized in Figure 3. The 'filling station' works by trapping a known amount of $CO_2$ gas in a cylinder of known volume at room temperature and relatively low pressure, the amount required for a given experiment is then transferred into the high-pressure tube by cryogenic pumping using liquid-$N_2$.

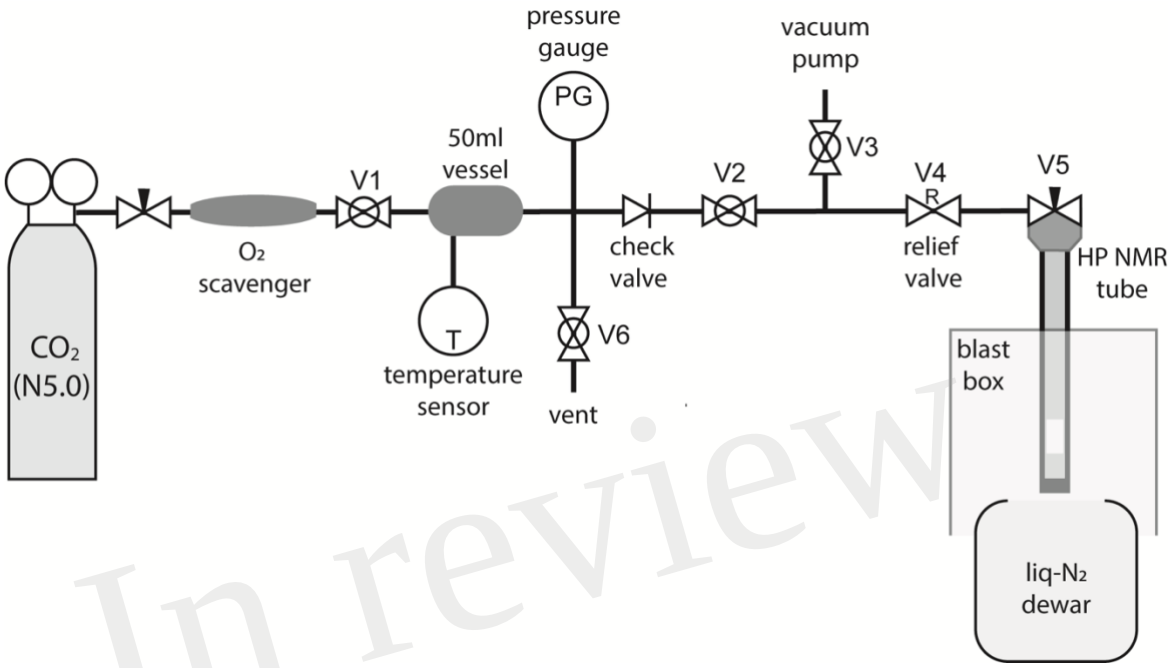


*Figure 3. A diagram of the custom-made $CO_2$ filling station built to fill high-pressure NMR tubes with liquid-$CO_2$*

The gas from a N5.0 grade $CO_2$ canister fills a 50 ml vessel at the desired pressure as monitored through a pressure sensor connected to the vessel. The vessel is at room temperature and the exact value of the temperature is measured and noted. The $O_2$ content of the $CO_2$ bottle has been measured to be 1 ppb using a OxyQC Wide Range oxygen meter by Anthon Paar; the gas was nevertheless filtered through a Restek high-capacity oxygen and moisture trap placed between the bottle and the 50 ml vessel to further remove $O_2$. The whole tubing (including vessel and high-pressure tube) is filled with $CO_2$ and evacuated a few times to remove the $O_2$ possibly present in the equipment.

Successively, the desired amount of $CO_2$ gas at the desired pressure is trapped in the 50 ml vessel, from where it is sucked into the high-pressure NMR tube (which already contains a given amount of the desired molecular system) by immersing the tube into the liquid-nitrogen Dewar. The $CO_2$ gas liquifies or solidifies, depending on the exact conditions, inside the high-pressure tube and while under liquid-$N_2$. Once the transfer occurs, the NMR tube needle valve is closed, and the tube is left to equilibrate at ambient temperature. The amount of gas needed to be trapped in the 50 ml vessel ($V_V$ = 50 ml) is calculated on the basis of what amount of liquid-$CO_2$ we want/need to fill the high-pressure tube with[40]. In the preparations below where the high-pressure 10 mm sapphire tube is used, and similarly for the 5 mm zirconia case, our aim is to fill a 10.5 mm long and 5.8 mm ID chamber with liquid-$CO_2$ (details in Figure 2). To do that we calculate the volume of liquid $CO_2$ ($V_{liq}$) as a function of the mass of $CO_2$ ($M_{CO_2}$) to be trapped in that volume using:

$$V_{liq} = \frac{M_{CO_2}\ \chi_{liq}}{\rho_{liq}} \qquad (1)$$

where $\rho_{liq}$ is the density of liquid-$CO_2$ at the measured temperature (T) and the liquid fraction $\chi_{liq}$ is calculated once the density of liquid-$CO_2$, the density of gas-$CO_2$ ($\rho_{gas}$) and the system density ($\rho_{sys}$) are known:

$$\chi_{liq} = 1 - \frac{\rho_{gas}}{\rho_{sys}}\left(\frac{\rho_{liq}-\rho_{sys}}{\rho_{liq}-\rho_{gas}}\right) \quad (2)$$

$$\rho_{sys} = \frac{M_{CO_2}}{V_t} \quad (3)$$

$V_t$ is the total free volume in the tube which is the sum of the free volume of the chamber sitting in the middle of the coil plus the free volume in the gap between the tube inner walls and the insert. Since T, $\rho_{gas}$, $\rho_{liq}$ and $V_t$ are known we can set $V_{liq}$ to match (or better to slightly exceed) the volume of the chamber placed in the NMR coil ($V_C$) and therefore work out the mass of $CO_2$ required. This mass is then calculated through the perfect gas law as:

$$M_{CO_2} = \frac{MW_{CO_2}\, P\, V_V}{R\, T} \quad (4)$$

where R is the gas constant, P the pressure inside the vessel measured in our apparatus, and $MW_{CO_2}$ the molecular weight of the gas. The required mass of $CO_2$ is then dispensed by adjusting the pressure inside the 50 ml vessel. The value of the pressure for the preparation below typically ranges between 2 and 8 bars. For practical purposes it was advantageous to charge an additional 2 bars of $CO_2$ (over the calculated value) into the 50ml vessel. This ensured that when the required $CO_2$ was removed from the vessel air was prevented from being drawn in, in the case of a leak, the apparatus remaining under a 2 bars pressure.

As an illustrative example, to prepare sample **NapCo2e** in our 10 mm high-pressure sapphire tube with insert (see Figure 2) we have firstly calculated the tube free volume $V_t = 1098$ $\mu$l from known dimensions. Then, from tabulated values, we read $\rho_{gas} = 0.1942$ g/ml and $\rho_{liq} = 0.7734$ g/ml at the room temperature of 20 ºC. In this way, the mass of $CO_2$ that can be trapped in the 50 ml vessel at a pressure of 4.8 bar is $M_{CO_2} = 0.293$ g which gives a $\rho_{sys} = 0.394$ g/ml. This value is below the critical value and therefore the NMR tube will contain a mixture of liquid and gas. The volume of the liquid is calculated from Eq. 1 to be $V_{liq} = 380$ $\mu$l. Since the volume of the 10.5 mm chamber in the middle of the coil is $V_C = 280$ $\mu$l, then the amount of liquid-$CO_2$ would fill the chamber and the gap above and below it for a few centimeters. To reach the concentration of 50 mM for this sample, we have inserted 7.9 mg of **Nap** (MW = 426.36 g mol$^{-1}$). As discussed above we have therefore filled the 50 ml chamber with 6.8 bar of $CO_2$ gas and then transferred the gas into the NMR tube until the pressure reading was 2 bars.

Once the sample equilibrates at room temperature (20 ºC in our case), the approximate pressure inside the NMR tube can be estimated from the pressure-density phase diagrams of pure $CO_2$[40] to be ~54 bars which is well within the tubes' tolerances (the value is only approximate because the phase diagram of our exact mixture is not available). Samples are moved around the laboratory within custom-made polycarbonate blast boxes and personnel wear face shields and gloves until the tube is safely placed into the probe.

## 2.6 NMR procedures

All longitudinal decay constants ($T_1$) reported in this paper have been measured with a standard inversion recovery experiment. To measure single order decay constants ($T_S$) we have used a sequence (Figure 4) where firstly any singlet order possibly present in the sample from the previous scan is destroyed[41], singlet order is subsequently produced with either a M2S[42] or gM2S[43] pulse

sequence, depending on the actual spin system features. The singlet order is then allowed to relax in a specific magnetic field for some variable delay time before being reconverted back into transverse magnetization by a S2M or gS2M and acquired. A singlet filter block is inserted before the S2M/gS2M to filter through only singlet order. All measurements at fields below 7 T were performed in a field-cycling mode using a custom-made sample shuttle[28]. In these experiments the sample is (*i*) polarized in high field; (*ii*) magnetisation inverted with a 180 degrees pulse (for $T_1$) or converted to singlet order with a M2S or gM2S (for $T_S$); (*iii*) sample is moved to a region of lower field along the magnet vertical stray field where longitudinal or singlet order are let to decay; (*iv*) after a variable amount of time the sample is shuttled back into high field where a 90 degrees pulse (for $T_1$) or a S2M or gS2M are (for $T_S$) is applied before signal detection.

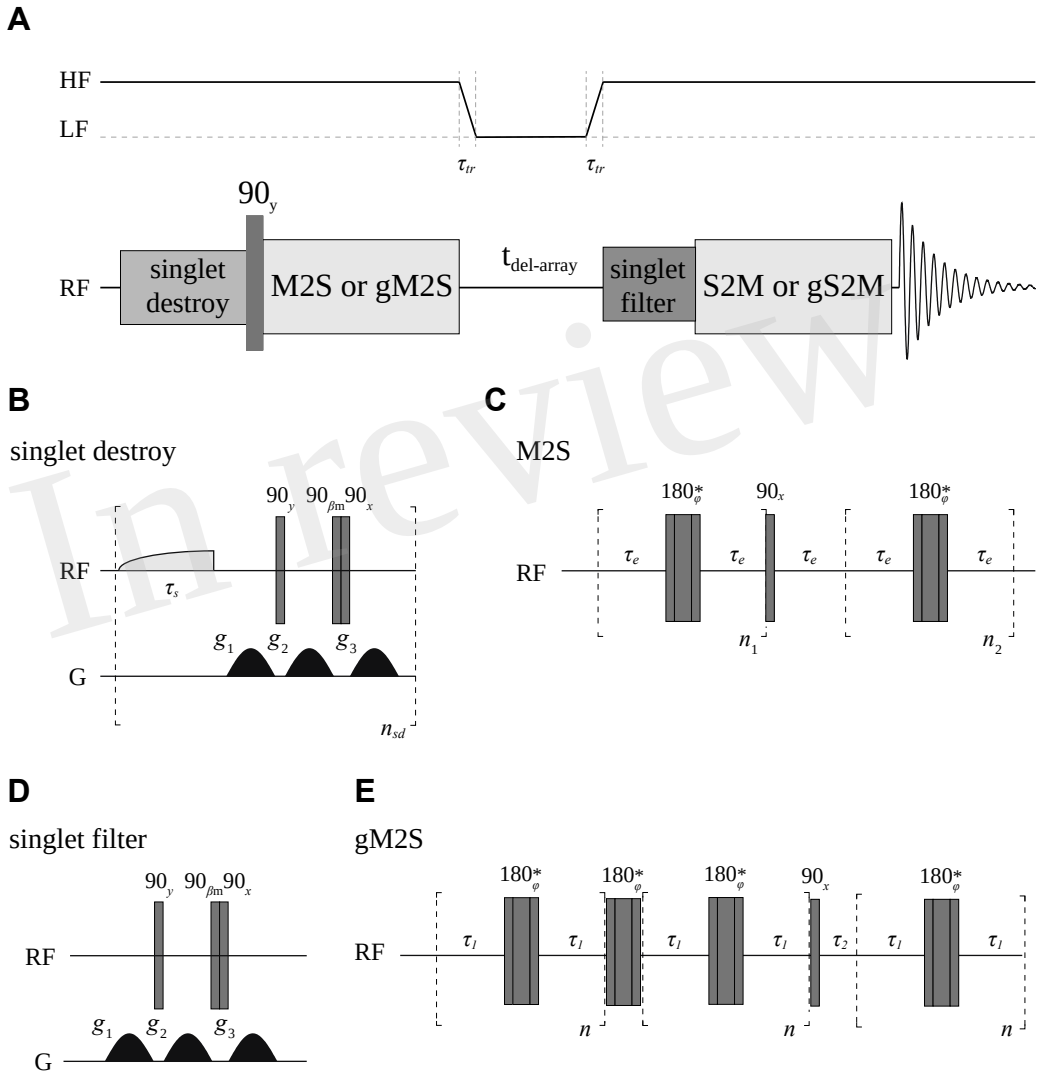


*Figure 4. A) Pulse sequence used to measure $T_S$ with details of the singlet-destroy scheme (B), M2S (C), $T_{00}$-filter (D) and gM2S (E) blocks. The S2M and gS2M blocks are the time-reverse of M2S and gS2M, respectively. The asterisk indicates a composite 180° pulse built as 90x180y90x. The phase φ is cycled as [x,x,-x,-x,-x,x,x,- x,-x,-x,x,x,x,-x,-x,x] within the train of 180° pulses. All gradients have half-sinusoidal shape and $\beta_m = \arctan(2^{1/2})$. The field variation indicated at the top of A is only used during the experiments run in field-cycling mode.*

The duration of a 90 degrees $^{13}C$ pulse was 11.2, 25.0 and 27.5 $\mu$s at 16.4, 11.7 and 7 T, respectively whereas the duration of the 90 degrees $^{1}H$ pulse was 9.5 $\mu$s at 7 T. Typically, for $^{13}C$ $T_1$ and $T_S$ experiments 8k points were collected using a 20kHz spectral window. The recycling delay was fixed to $5T_1$. The number of transients was set to 2 for all $T_1$ measurements and for $T_1$ and $T_S$ of **Mal**, **Act** and **Nap** in organic solvents whereas we have used 4 transients for $T_S$ measurements of Act and Nap in liquid-$CO_2$. The values of all parameters featuring in the pulse sequence of Figure 4

have been optimized around their theoretical values and the results are summarized in Table 2. The gradients featuring in the singlet filter are applied along the z-axis and have strength of 75, -75 and -75 mT $m^{-1}$ and durations of 2.4, 1.4 and 1 ms, respectively. The singlet destroy scheme has been implemented using a qramp shaped pulse of duration $\tau_s$ = 1 s and maximum nutation frequency of 400 Hz. The sequence "shaped pulse-singlet filter" has been repeated $n_{sd}$ = 5 times. In all field-cycling experiments the sample transport time $\tau_{tr}$ was set to 4 s.

*Table 2. Experimental values of the pulse sequence parameters used for the various samples in measuring $T_S$ with the pulse sequence in Figure 4.*

| Sample | 7 T | | | 11.7 T | | | 16.4 T | | |
|---|---|---|---|---|---|---|---|---|---|
| | $n_1$ | $n_2$ | $\tau_e$(ms) | $n_1$ | $n_2$ | $\tau_e$(ms) | $n_1$ | $n_2$ | $\tau_e$(ms) |
| **NapTbu** | 14 | 7 | 4.6 | 8 | 4 | 4.6 | 6 | 3 | 4.6 |
| **NapDms** | 28 | 14 | 4.6 | 16 | 8 | 4.6 | 12 | 6 | 4.6 |
| **NapEth** | 16 | 8 | 4.6 | 10 | 5 | 4.6 | 6 | 3 | 4.6 |
| **NapClf** | 16 | 8 | 4.6 | 10 | 5 | 4.6 | 6 | 3 | 4.6 |
| **NapMet** | 16 | 8 | 4.6 | 10 | 5 | 4.6 | 6 | 3 | 4.6 |
| **NapAce** | 20 | 10 | 4.6 | 12 | 6 | 4.6 | 8 | 4 | 4.6 |
| **NapCo2e** | 22 | 11 | 4.6 | 12 | 6 | 4.6 | 8 | 4 | 4.6 |

| | $n_1$ | $n_2$ | $\tau_e$(ms) |
|---|---|---|---|
| **MalEth** | 20 | 10 | 20.9 |
| **MalCo2** | 44 | 22 | 20.9 |

| | n | $\tau_1$(ms) | $\tau_2$(ms) |
|---|---|---|---|
| **ActClf** | 3 | 1.10 | 0.7 |
| **ActCo2** | **3** | 1.12 | 1.20 |



# 3 Experimental

## 3.1 Naphthalene derivative (Nap)

The naphthalene derivative[37] (**Nap**) was chosen for initial investigations to develop and test the proposed procedures. The choice is based on the extraordinary long lifetime of the singlet order in this custom-designed and synthesised molecule.[27, 28]

### 3.1.1 Concentration dependence of $T_1$ and $T_S$ in liquid-$CO_2$ solutions

The solubility of **Nap** in liquid-$CO_2$ was not known, nor it was known if sample concentration would affect the observed decay time. As a preliminary investigation a series of solutions of increasing concentrations of **Nap** in liquid-$CO_2$ at 20 ºC were prepared and $T_1$ and $T_S$ measured. Inspection of the results depicted in Figure 5 reveals no significant trend in $T_1$ or $T_S$ with increasing concentration, it was concluded that a working concentration of 50 mM **Nap** in liquid-$CO_2$ was reasonable.

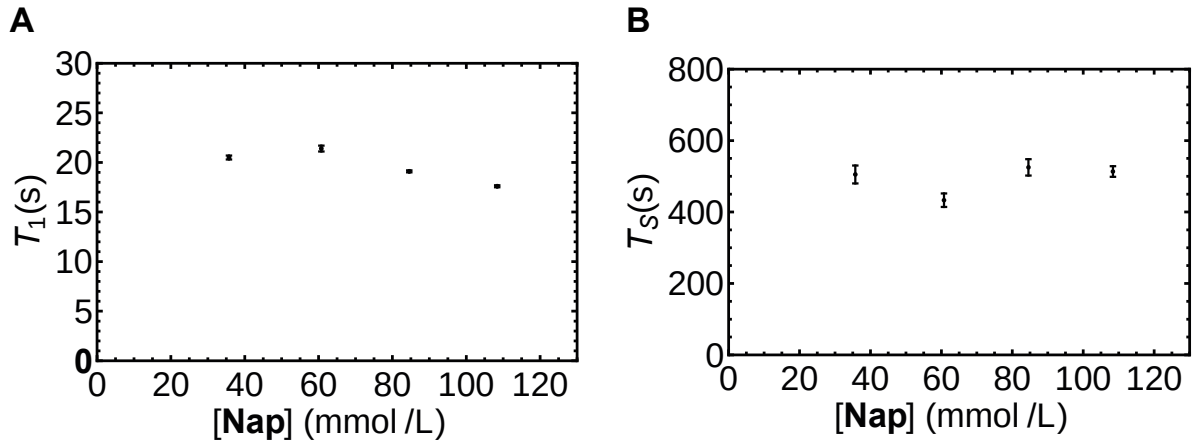


*Figure 5. $T_1$ (A) and $T_S$ (B) for **Nap** dissolved in liquid-$CO_2$ at different concentrations (samples **NapCo2a-d** in Table 1).*

### 3.1.2 Viscosity dependence of $T_1$ and $T_S$ in liquid-$CO_2$ solutions

To validate the initial hypothesis that both $T_1$ and $T_S$ can be prolonged in low-viscosity solutions, **Nap** was dissolved in a range of solvents of different viscosities from *tert*-butanol to liquid-$CO_2$. $T_1$ and $T_S$ were measured in samples **NapTbu**, **NapDms**, **NapEth**, **NapClf**, **NapMet**, **NapAce** and **NapCo2e** and results from these experiments are summarized in Figure 6. These measurements have been taken at three different magnetic fields: 7 (Figure 6a), 11.7 (Figure 6b) and 16.4 T (Figure 6c).

Both $T_1$ and $T_S$ correlate linearly with inverse viscosity in common organic solvents at all three field strengths. At 16.4 T, the values of $T_1$ and $T_S$ measured in liquid-$CO_2$ solution (**NapCo2e**) also demonstrated a linear relationship with viscosity. Deviation from this behavior is observed at lower fields (Figure 6A and B) where the values of $T_1$ and $T_S$ for **NapCo2e** fail to meet the predicted value (blue line), indicating that, although the values of $T_1$ and $T_S$ are significantly increased in liquid-$CO_2$, the time gain reduces as the magnetic field, at which relaxation occurs, reduces (Figure 6 and Table 3).

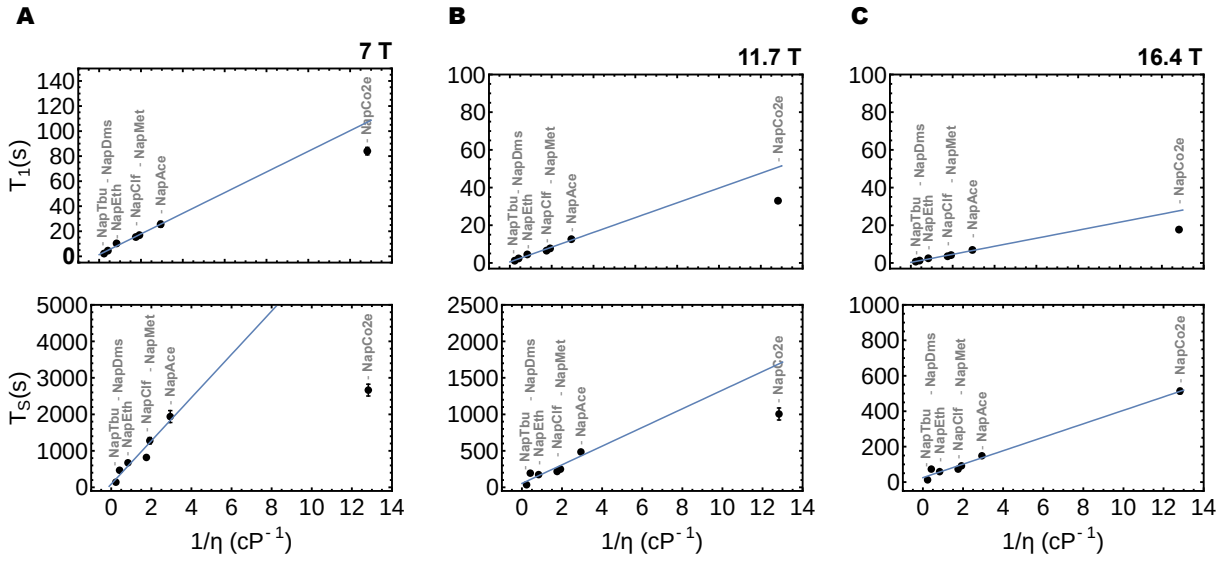


*Figure 6. $T_1$ and $T_S$ as a function of inverse viscosity in samples **NapTbu-NapCo2e** at 7, 11.7 and 16.4 Tesla fields in columns A, B and C, respectively. The blue line is the best fit to values for samples **NapTbu-NapAce***

### 3.1.3 Field dependence of $T_1$ and $T_S$ in liquid-$CO_2$ solutions

The trends observed in Figure 6 are evidence for the following: at the highest field, the relaxation of singlet order is dominated by chemical shift anisotropy, a mechanism whose contribution to the relaxation decay constant is directly proportional to inverse viscosity; as the field is lowered, the contribution to the relaxation rate from other mechanisms prevails, such mechanisms would therefore have a different proportionality to viscosity.

If this is the case, further reducing the field to a value where the chemical shift anisotropy contribution becomes negligible would make the $T_S$ in liquid-$CO_2$ fall below any recorded values. The same is not expected for $T_1$ as longitudinal order relaxation at any field would be dominated by the dipole-dipole mechanism whose contribution to the decay constant is inversely proportional to viscosity.

To investigate this hypothesis, we have measured the relaxation decay constants of longitudinal and singlet order at a range of fields between 50 mT and 7 T. Experiments were carried out in a field-cycling mode as described in Materials and Methods and for samples **NapEth, NapAce** and **NapCo2e** where the labelled molecule **Nap** is dissolved in ethanol-$d_6$, acetone-$d_6$ and liquid-$CO_2$, respectively.

*Table 3. $T_1$ and $T_S$ values for samples **NapEth**, **NapAce** and **NapCo2e** obtained at 20 °C and different magnetic field strengths*

| Field (T) | $T_1$ (s) | | | $T_S$ (s) | | |
|---|---|---|---|---|---|---|
| | NapEth | NapAce | NapCo2e | NapEth | NapAce | NapCo2e |
| 0.05 | 26 ± 2 | 72 ± 3 | 135 ± 26 | 1350 ± 98 | 5319 ± 682 | 4553 ± 470 |
| 0.10 | 33 ± 5 | 75 ± 5 | 126 ± 18 | 1587 ± 130 | 4454 ± 369 | * |
| 0.25 | 25 ± 1 | 92 ± 11 | 176 ± 12 | 1573 ± 70 | 4460 ± 369 | 3785 ± 318 |
| 0.5 | 30 ± 4 | 80 ± 5 | 158 ± 14 | 1503 ± 52 | 5146 ± 484 | 3266 ± 192 |
| 1 | 32 ± 3 | 80 ± 8 | 148 ± 20 | 1426 ± 76 | 5075 ± 363 | 3171 ± 153 |
| 2 | 30 ± 4 | 70 ± 10 | 175 ± 18 | 1556 ± 21 | 4429 ± 381 | * |
| 3 | 27 ± 1 | 57 ± 3 | 122 ± 7 | 1291 ± 62 | 3852 ± 302 | 2851 ± 105 |
| 7 | 10 ± 1 | 30 ± 1 | 84 ± 3 | 620 ± 30 | 1621 ± 208 | 2664 ± 161 |
| 11.7 | 4.5 ± 0.1 | 16 ± 1 | 33 ± 1 | 174 ± 2 | 485 ± 16 | 1005 ± 82 |
| 16.4 | 2.5 ± 0.1 | 7 ± 0.2 | 18 ± 0.1 | 59 ± 1 | 148 ± 5 | 513 ± 15 |

* Data not collected

Close examination of the results of the field-cycling experiments (Table 3) reveals that for $T_1$, as the time increased the field decreased (in all samples) indicating that the chemical shift anisotropy relaxation mechanism has a fundamental contribution to the observed decay constant at high field. However, at lower fields the $T_1$ values in liquid-$CO_2$ (**NapCo2e**) are significantly longer than those recorded in both ethanol-$d_6$ (**NapEth**) and acetone-$d_6$ (**NapAce**). The values of $T_1$ measured in liquid-$CO_2$ compared to ethanol-$d_6$ are extended by a factor of ~7 at relatively high fields (16.4 - 7 T) but at lower fields this factor reduces to ~5. When considering the sample in acetone-$d_6$.the extension factor is ~2 at all fields.

A similar trend can be seen for $T_S$. The $T_S$ in liquid-$CO_2$ remains significantly longer than that measured in ethanol-$d_6$ at all fields, whereas in acetone-$d_6$, only at high fields is the value of $T_S$ is longer in liquid-$CO_2$.

Interpreting our observations in a qualitative way, at high field, $T_1$ is dominated mainly by the interplay of ipDD and CSA mechanisms so the value of $T_1$ increases as the CSA is progressively suppressed by transporting the sample to relax in a lower field. The contribution to the relaxation rate of both these mechanisms is expected to decrease as the viscosity reduces explaining the significantly longer decay constants in liquid-$CO_2$ with respect to ethanol-$d_6$. The fall in lifetime extension of the liquid-$CO_2$ sample in comparison to ethanol-$d_6$ and acetone-$d_6$ as the field is lowered is due to the presence of a mechanism whose contribution becomes more relevant once the CSA becomes of less importance. The explanation is similar for the $T_S$ data, however, since singlet order is immune to the ipDD mechanism, at high field the singlet order relaxation is mainly dominated by CSA whilst, other mechanisms become more important at lower field.

## 3.2 Acetylene derivative (Act)

The field-cycling study to measure $T_1$ and $T_S$ as a function of magnetic field where relaxation occurs was repeated for the singlet-bearing acetylene derivative **Act** dissolved in $CDCl_3$ (**ActClf**) and in liquid-$CO_2$ (**ActCo2**) for comparison. Results from this study are summarized in Table 4.

*Table 4. $T_1$ and $T_S$ values for samples **ActClf** and **ActCo2** obtained at 20 ºC and different magnetic field strengths*

| Field (T) | $T_1$ (s) | | $T_S$ (s) | |
|---|---|---|---|---|
| | ActClf | ActCo2 | ActClf | ActCo2 |
| 0.05 | 34 ± 1 | 96 ± 2 | 4123 ± 260 | 2605 ± 258 |
| 0.10 | 32 ± 1 | 102 ± 9 | 3675 ± 320 | * |
| 0.25 | 36 ± 2 | 127 ± 6 | 3077 ± 300 | * |
| 0.5 | 37 ± 2 | 120 ± 5 | 2914 ± 156 | 2611 ± 82 |
| 1 | 41 ± 1 | 146 ± 12 | 1468 ± 56 | 2450 ± 120 |
| 3 | 47 ± 3 | 132 ± 8 | 214 ± 20 | 805 ± 78 |
| 5 | 35 ± 2 | 114 ± 6 | 100 ± 8 | * |
| 7 | 20 ± 1 | 78 ± 3 | 54 ± 6 | 218 ± 17 |

* Data not collected

Again, both $T_1$ and $T_S$ increased as the field decreased, once more pointing towards a substantial role of CSA in the relaxation mechanism at high field. However, the $T_1$ reaches a maximum at 3T and then slowly diminishes again towards lower fields. There is a clear time gain of a factor of 3-4 approximately in longitudinal order lifetime when using liquid-$CO_2$ as a solvent in comparison to $CDCl_3$. Interestingly, $T_S$ shows a significant gain of a factor of ~4 in liquid-$CO_2$ (from 7 T down to 3 T) but this factor diminishes and even inverts at lower fields, with the $T_S$ in $CDCl_3$ being longer than that measured in liquid-$CO_2$ in very low field.

## 3.3 Maleate derivative (Mal)

In a third set of field-cycling experiments the $T_1$ and $T_S$ of molecule **Mal** was measured at a range of magnetic fields both in ethanol-$d_6$ (**MalEth**) and liquid-$CO_2$ (**MalCo2**). Results from this study are summarized in Table 5. In this sample the singlet order is created in the proton spin-pair and protons have notoriously much smaller chemical shift tensors than carbons. For this reason, it is not expected that the CSA relaxation mechanism contributes significantly to the total relaxation decay at any magnetic field. Indeed, from the data in the table the values of both $T_1$ and $T_S$ in either sample do not vary significantly as the field is lowered. Comparing the results in liquid-$CO_2$ with those in ethanol-$d_6$, a gain by a factor ~4 is observed for $T_1$ but there is a more modest gain factor of ~1.4 observed for $T_S$.

*Table 5. $T_1$ and $T_S$ values for samples **MalEth** and **MalCo2** obtained at 20 ºC and different magnetic field strengths*

| Field (T) | $T_1$ (s) | | $T_S$ (s) | |
|---|---|---|---|---|
| | MalEth | MalCo2 | MalEth | MalCo2 |
| 0.05 | 9.6 ± 0.1 | 37.6 ± 0.4 | 237 ± 2 | 294 ± 8 |
| 0.10 | 9.5 ± 0.2 | 37.6 ± 0.3 | 233 ± 2 | 325 ± 20 |
| 0.25 | 9.7 ± 0.2 | 39.2 ± 0.4 | 251 ± 4 | 327 ± 15 |
| 0.5 | 9.7 ± 0.2 | 39.4 ± 0.5 | 249 ± 6 | 344 ± 22 |
| 1 | 9.8 ± 0.2 | 41.2 ± 0.3 | 250 ± 6 | 376 ± 21 |
| 3 | 9.5 ± 0.1 | 43.8 ± 0.5 | 246 ± 9 | 364 ± 15 |
| 5 | 9.8 ± 0.1 | 44.3 ± 0.8 | 237 ± 8 | 331 ± 15 |
| 7 | 9.7 ± 0.1 | 43.8 ± 1.6 | 242 ± 6 | 359 ± 27 |

# 4 Discussion

The data presented above can be interpreted using a relaxation analysis based on previously derived analytical equations for the contribution of different mechanisms to the total relaxation rate of singlet spin order[1, 44]. To do so, it is better to discuss in terms of decay rates $R_1 = 1/T_1$ and $R_S = 1/T_S$ since the contributions of different relaxation mechanisms to the rate is additive. Additionally, we are going to use a simplified model where only the intrapair dipole-dipole (ipDD), chemical shift anisotropy (CSA) and the coherent chemical shift leak (CSL) mechanism are explicitly introduced. The remaining contribution to the total decay rate will be introduced as an unknown mechanism and its value retrieved through data fitting.

The equations for the decay rates due to the cited mechanism have been largely discussed in literature[1] and are reported here for convenience:

$$
\begin{aligned}
&R_1^{\mathrm{ipDD}} = \tfrac{3}{2} b_{jk}^2 \tau_2; && R_S^{ipDD} = 0 \\
&R_1^{CSA^+} = \tfrac{1}{10}\gamma^2 B_0^2 \tau_2 \left( \left\| \boldsymbol{\delta_j^+} \right\|^2 + \left\| \boldsymbol{\delta_k^+} \right\|^2 \right); && R_S^{CSA^+} = \tfrac{2}{9}\gamma^2 B_0^2 \tau_2 \left\| \boldsymbol{\delta_j^+} - \boldsymbol{\delta_k^+} \right\|^2 \\
&R_1^{CSA^-} = \tfrac{1}{6}\gamma^2 B_0^2 \tau_1 \left( \left\| \boldsymbol{\delta_j^-} \right\|^2 + \left\| \boldsymbol{\delta_k^-} \right\|^2 \right); && R_S^{CSA^-} = \tfrac{2}{9}\gamma^2 B_0^2 \tau_1 \left\| \boldsymbol{\delta_j^-} - \boldsymbol{\delta_k^-} \right\|^2 \qquad (5) \\
&R_1^{CSL} = 0; && R_S^{CSL} = \frac{\gamma^2 B_0^2 \Delta\delta_{iso}^2 \tau_2 b_{jk}^2}{12\pi^2 J_{jk}^2}
\end{aligned}
$$

where $b_{jk} = -\hbar\mu_0\gamma^2/(4\pi r_{jk}^3)$ and $J_{jk}$ are, respectively, the dipolar and indirect coupling constants between the two nuclei in the singlet spin-pair; $B_0$ is the static magnetic field, $\Delta\delta_{iso} = \delta_j - \delta_k$ is the difference in the chemical shift of the two nuclei; $\tau_1$ and $\tau_2$ are the correlation times for rank-1 and rank-2 mechanisms, respectively and with $\tau_1 = 3\,\tau_2$; $\gamma$ is the gyromagnetic ratio; $\boldsymbol{\delta}^+$and $\boldsymbol{\delta}^-$ are the symmetric (+) and asymmetric (-) parts of the chemical shift tensor for the two nuclei in the singlet pair; $\|\boldsymbol{\delta}\|$ indicates the Frobenius norm of the tensor $\boldsymbol{\delta}$.

The strategy adopted is based on the following assumptions:

- $T_1$ in low field is dominated by the ipDD mechanism only, thus we can use $R_1^{\mathrm{ipDD}}$ and the experimental value of $T_1$ at 50 mT to retrieve the correlation time (other spin system parameters reported in Table 6)

$$\tau_2 = \frac{2}{3 b_{jk}^2 T_1(50\mathrm{mT})} \qquad (6)$$

- $T_1$ at any other field is due to the effect of ipDD and CSA mechanisms:

$$T_1 = 1/(R_1^{\mathrm{ipDD}} + R_1^{CSA^+} + R_1^{CSA^-}) \qquad (7)$$

- $T_S$ at all fields is due to the combination of CSA and CSL terms plus a further mechanism whose rate $R_S^{\mathrm{X}}$ will be determined by fitting the experimental $T_S$:

$$T_S = 1/(R_S^{CSA^+} + R_S^{CSA^-} + R_S^{\mathrm{CSL}} + R_S^{\mathrm{X}}) \qquad (8)$$

In the case of sample **NapAce** and using Eq. 6 we find a correlation time $\tau_2 = 31$ ps which can then be used to predict the value of $T_1$ and $T_S$ at any field. The values of $T_1$ predicted using Eq. 7 are plotted as a continuous line in Figure 7A and overlapped with the experimental point of Table 3 for an easy comparison. In the case of $T_S$ we have fitted the experimental data against Eq. 8 and for the unknown $R_S^{\mathrm{X}}$ which was found to be $198.5 \times 10^{-6}$ s$^{-1}$. The fitting is shown in Figure 7B.

*Table 6. Parameters used in the relaxation analysis for the case of **NapAce** and **NapCo2e**. Chemical shift tensors have been calculated in Ref. [27] and here are assumed identical for both samples.*

| Parameter | NapAce | NapCo2e |
|---|---|---|
| $r_{jk}$ | 1.395 Å | 1.395 Å |
| $J_{jk}$ | 54.8 Hz | 54.8 Hz |
| $\Delta\delta_{iso}$ | 0.057 ppm | 0.052 ppm |
| $\|\boldsymbol{\delta}_j^+\|$ | 107 ppm | |
| $\|\boldsymbol{\delta}_k^+\|$ | 112 ppm | |
| $\|\boldsymbol{\delta}_j^-\|$ | 2.6 ppm | |
| $\|\boldsymbol{\delta}_k^-\|$ | 8.1 ppm | |
| $\|\boldsymbol{\delta}_j^+ - \boldsymbol{\delta}_k^+\|$ | 6.7 ppm | |
| $\|\boldsymbol{\delta}_j^- - \boldsymbol{\delta}_k^-\|$ | 9.9 ppm | |

The same procedure was used to predict the values of $T_1$ and $T_S$ for the sample of **Nap** in liquid-$CO_2$ (**NapCo2e**). In this case and using Eq. 6 we found a value of the correlation time of $\tau_2 = 16$ ps and the fitted value of $R_S^X$ was found to be $268.3 \times 10^{-6}$ s$^{-1}$. The predicted values for this case are shown in Figure 7C and D for $T_1$ and $T_S$, respectively.

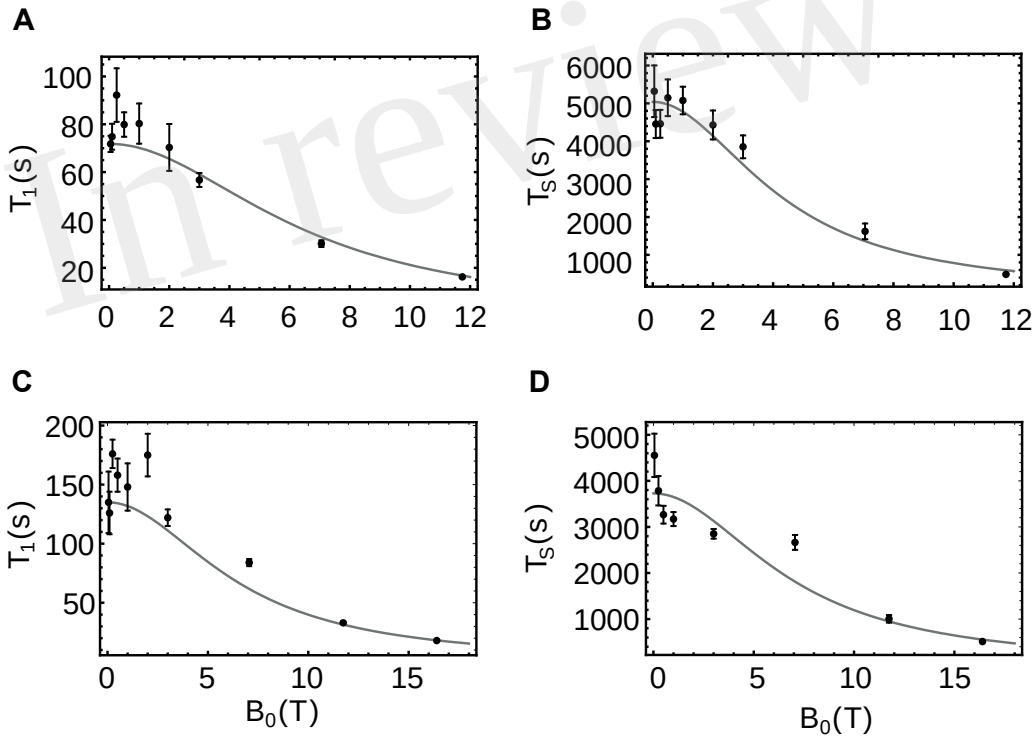


*Figure 7. Filled circles are the values of $T_1$ and $T_S$ experimentally measured for samples **NapAce** (A, B) and **NapCo2e** (C, D), also available in Table 3. The gray curves are the predicted values of these decay constants obtained using Eqs. 5-8.*

The results of this approximate relaxation analysis can be summarized as follows: in agreement with the initial hypothesis, the $T_1$ of these samples is essentially defined by the ipDD and CSA relaxation terms since the predicted values matches well the experimental points; in the case of $T_S$, relaxation in low fields is governed by a mechanism that contributes with a rate of $195.5 \times 10^{-6}$ for the case of **Nap** in acetone-$d_6$ and $268.3 \times 10^{-6}$ for the case of **Nap** in liquid-$CO_2$. This additional mechanism seems to have less dependence on viscosity than ipDD or CSA since its value is higher in the less viscous liquid-$CO_2$ sample. One possible candidate is the spin-rotation mechanism whose dependence on the solvent viscosity is opposite to that of ipDD and CSA. Besides, this mechanism, its variant known as spin-internal motion (SIM), has already been

proposed as an important relaxation mechanism for the singlet spin order of **Nap** in a previous study[27].

## 5 Conclusion

In this study we have run a thorough investigation of the lifetime of both longitudinal and singlet order decay times of three different molecules in liquid-$CO_2$ solutions in comparison with the values measured in more *common* organic solvents. The motivation behind this work was the concept that longitudinal and singlet order lifetimes could be extended in low viscosity compressed gases in comparison to solvents which are liquid at ordinary pressures and temperatures. Significantly, we have shown that liquid-$CO_2$ allows an extension of lifetime of at least 2-fold when compared with lifetime available in acetone-$d_6$, one of the lowest viscosity solvents available. However, and depending on the relaxation mechanisms acting, such gain may not be able to prolong the absolute lifetime of singlet order since the latter hits a plateau where relaxation seems to be dominated by mechanisms that do not necessarily benefit from the lower viscosity of the liquid-$CO_2$ solution.

Nevertheless, the possibility to store spin polarization (and hence hyperpolarization) for as long as 76 minutes, in the case of **NapCo2e,** at 50 mT, but in a solvent which can be removed almost instantaneously by simply opening the tube, suggests the possibility of new exciting experiments. Experiments where hyperpolarization is stored for tens of minutes in a substrate dissolved in liquid-$CO_2$ and retrieved, at the time of use, by quick evaporation followed by dissolution in an experiment-compatible solvent which is perhaps not very convenient for hyperpolarization storage. We are currently building equipment to verify this hypothesis.



## Author contributions

AM, FG and AMRH have equally contributed to this paper. AM and TAAC ran experiments and processed data; FG built the $CO_2$ equipment and provided engineering support; AMRH built the sample shuttle, run experiments and processed data; LJB synthesised the molecules and provided chemical support. GP devised the research, ran some experiments and wrote the paper.

## Acknowledgments

We thank Pär Håkansson for providing computational data.

## Funding

This research was supported by EPSRC grant no. EP/P005187/1.

## Conflict of Interest

The authors declare that the research was conducted in the absence of any commercial or financial relationships that could be construed as a potential conflict of interest.

## References:

1. G. Pileio, ed., *Long-lived Nuclear Spin Order: Theory and Applications*, Royal Society of Chemistry, London, 2020.
2. M. Carravetta and M. H. Levitt, *J. Am. Chem. Soc.*, 2004, **126**, 6228-6229.
3. M. Carravetta, O. G. Johannessen and M. H. Levitt, *Phys. Rev. Letters*, 2004, **92**, 153003.
4. R. Buratto, D. Mammoli, E. Chiarparin, G. Williams and G. Bodenhausen, *Angewandte Chemie International Edition*, 2014, **53**, 11376-11380.
5. N. Salvi, R. Buratto, A. Bornet, S. Ulzega, I. Rentero Rebollo, A. Angelini, C. Heinis and G. Bodenhausen, *Journal of the American Chemical Society*, 2012, **134**, 11076-11079.
6. M. C. Tourell, I.-A. Pop, L. J. Brown, R. C. D. Brown and G. Pileio, *Physical Chemistry Chemical Physics*, 2018, **20**, 13705-13713.
7. G. Pileio and S. Ostrowska, *J Magn Reson*, 2017, **285**, 1-7.

8. G. Pileio, J.-N. Dumez, I.-A. Pop, J. T. Hill-Cousins and R. C. D. Brown, *Journal of Magnetic Resonance*, 2015, **252**, 130-134.
9. J. N. Dumez, J. T. Hill-Cousins, R. C. D. Brown and G. Pileio, *Journal of Magnetic Resonance*, 2014, **246**, 27-30.
10. P. Ahuja, R. Sarkar, P. R. Vasos and G. Bodenhausen, *Journal of the American Chemical Society*, 2009, **131**, 7498-7499.
11. S. Cavadini, J. Dittmer, S. Antonijevic and G. Bodenhausen, *Journal of the American Chemical Society*, 2005, **127**, 15744-15748.
12. P. Saul, S. Mamone and S. Glöggler, *Chem Sci*, 2019, **10**, 413-417.
13. S. Yang, J. McCormick, S. Mamone, L. S. Bouchard and S. Glöggler, *Angew Chem Int Ed Engl*, 2019, **58**, 2879-2883.
14. C. P. N. Tanner, J. R. Lindale, S. L. Eriksson, Z. Zhou, J. F. P. Colell, T. Theis and W. S. Warren, *J Chem Phys*, 2019, **151**, 044201.
15. S. Mamone and S. Glöggler, *Phys Chem Chem Phys*, 2018, **20**, 22463-22467.
16. T. Theis, G. X. Ortiz, A. W. Logan, K. E. Claytor, Y. Feng, W. P. Huhn, V. Blum, S. J. Malcolmson, E. Y. Chekmenev, Q. Wang and W. S. Warren, *Sci Adv*, 2016, **2**, e1501438.
17. J.-N. Dumez, P. Håkansson, S. Mamone, B. Meier, G. Stevanato, J. T. Hill-Cousins, S. S. Roy, R. C. D. Brown, G. Pileio and M. H. Levitt, *The Journal of Chemical Physics*, 2015, **142**, 044506.
18. Y. Feng, T. Theis, X. Liang, Q. Wang, P. Zhou and W. S. Warren, *J Am Chem Soc*, 2013, **135**, 9632-9635.
19. S. J. DeVience, R. L. Walsworth and M. S. Rosen, *NMR in Biomedicine*, 2013, n/a-n/a.
20. Y. Zhang, X. Duan, P. C. Soon, V. Sychrovský, J. W. Canary and A. Jerschow, *Chemphyschem*, 2016, **17**, 2967-2971.
21. Y. Zhang, K. Basu, J. W. Canary and A. Jerschow, *Phys Chem Chem Phys*, 2015, **17**, 24370-24375.
22. Y. N. Zhang, P. C. Soon, A. Jerschow and J. W. Canary, *Angewandte Chemie-International Edition*, 2014, **53**, 3396-3399.
23. C. R. Bowers and D. P. Weitekamp, *J. Am. Chem. Soc.*, 1987, **109**, 5541-5542.
24. R. W. Adams, J. A. Aguilar, K. D. Atkinson, M. J. Cowley, P. I. Elliott, S. B. Duckett, G. G. Green, I. G. Khazal, J. López-Serrano and D. C. Williamson, *Science*, 2009, **323**, 1708-1711.
25. J. H. Ardenkjaer-Larsen, B. Fridlund, A. Gram, G. Hansson, L. Hansson, M. H. Lerche, R. Servin, M. Thaning and K. Golman, *Proc. Natl. Acad. Sci. USA*, 2003, **100**, 10158-10163.
26. D. Gajan, A. Bornet, B. Vuichoud, J. Milani, R. Melzi, H. A. van Kalkeren, L. Veyre, C. Thieuleux, M. P. Conley, W. R. Grüning, M. Schwarzwälder, A. Lesage, C. Copéret, G. Bodenhausen, L. Emsley and S. Jannin, *Proceedings of the National Academy of Sciences*, 2014, **111**, 14693-14697.
27. G. Stevanato, J. T. Hill-Cousins, P. Håkansson, S. S. Roy, L. J. Brown, R. C. D. Brown, G. Pileio and M. H. Levitt, *Angewandte Chemie International Edition*, 2015, **54**, 3740–3743.
28. A. M. R. Hall, T. A. A. Cartlidge and G. Pileio, *J Magn Reson*, 2020, **317**, 106778.
29. J. Kowalewski and L. Mäler, *Nuclear Spin Relaxation in Liquids: Theory, Experiments and Applications*, CRC Press, Boca Raton, Florida, 2006.
30. M. H. Levitt, *Annual Review of Physical Chemistry*, 2012, **63**, 89-105.
31. S. Gaemers, C. J. Elsevier and A. Bax, *Chemical Physics Letters*, 1999, **301**, 138-144.
32. S. Bai, C. M. V. Taylor, F. Liu, C. L. Mayne, R. J. Pugmire and D. M. Grant, *The Journal of Physical Chemistry B*, 1997, **101**, 2923-2928.
33. I. Khodov, A. Dyshin, S. Efimov, D. Ivlev and M. Kiselev, *Journal of Molecular Liquids*, 2020, **309**, 113113.
34. S. Gaemers and C. J. Elsevier, *Magnetic Resonance in Chemistry*, 2000, **38**, 650-654.
35. C. R. Yonker, *The Journal of Physical Chemistry A*, 2000, **104**, 685-691.
36. D. M. Lamb, S. T. Adamy, K. W. Woo and J. Jonas, *The Journal of Physical Chemistry*, 1989, **93**, 5002-5005.
37. J. T. Hill-Cousins, I. A. Pop, G. Pileio, G. Stevanato, P. Hakansson, S. S. Roy, M. H. Levitt, L. J. Brown and R. C. Brown, *Org Lett*, 2015, **17**, 2150-2153.
38. G. Pileio, J. T. Hill-Cousins, S. Mitchell, I. Kuprov, L. J. Brown, R. C. D. Brown and M. H. Levitt, *Journal of the American Chemical Society*, 2012, **134**, 17494-17497.
39. L. J. Brown, in *Long-lived nuclear spin order: theory and applications*, ed. G. Pileio, Royal Society of Chemistry, London, 2020, ch. 4.
40. R. Smith, H. Inmate and C. Peters, eds., *Introduction to supercritical fluids, a spreadsheets based approach*, Elsevier, The Netherlands, 2013.
41. B. A. Rodin, K. F. Sheberstov, A. S. Kiryutin, L. J. Brown, R. C. D. Brown, M. Sabba, M. H. Levitt, A. V. Yurkovskaya and K. L. Ivanov, *J Chem Phys*, 2019, **151**, 234203.
42. G. Pileio, M. Carravetta and M. H. Levitt, *Proceedings of the National Academy of Sciences of the United States of America*, 2010, **107**, 17135-17139.
43. C. Bengs, M. Sabba, A. Jerschow and M. H. Levitt, *Phys Chem Chem Phys*, 2020, **22**, 9703-9712.
44. G. Pileio, *Progress in Nuclear Magnetic Resonance Spectroscopy*, 2010, **56**, 217-231.

Figure 1.TIF

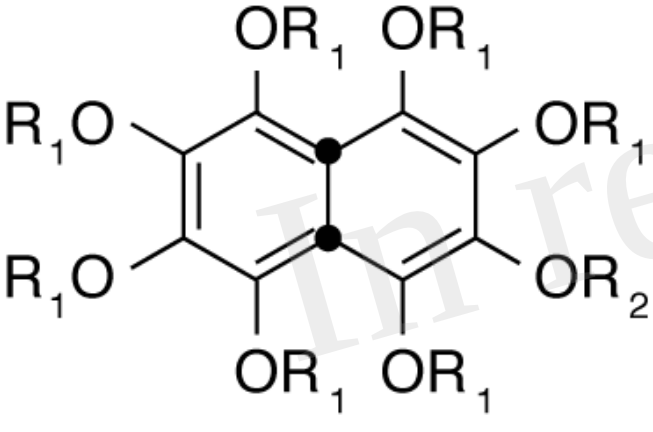


**(Nap)**

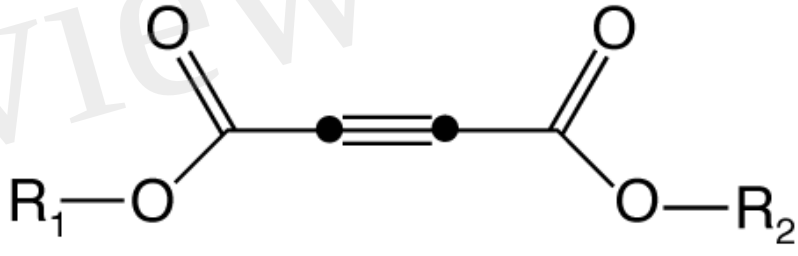


**(Act)**

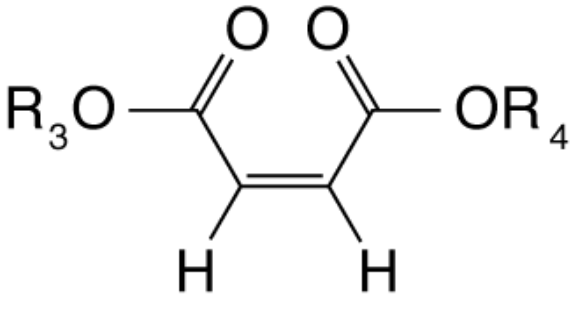


**(Mal)**

● denotes $^{13}C$

$R_1 = CD_3$

$R_2 = CD(CD_3)_2$

$R_3 = CD_2CD_3$

$R_4 = CD_2CD_2CD_3$

Figure 2.TIF

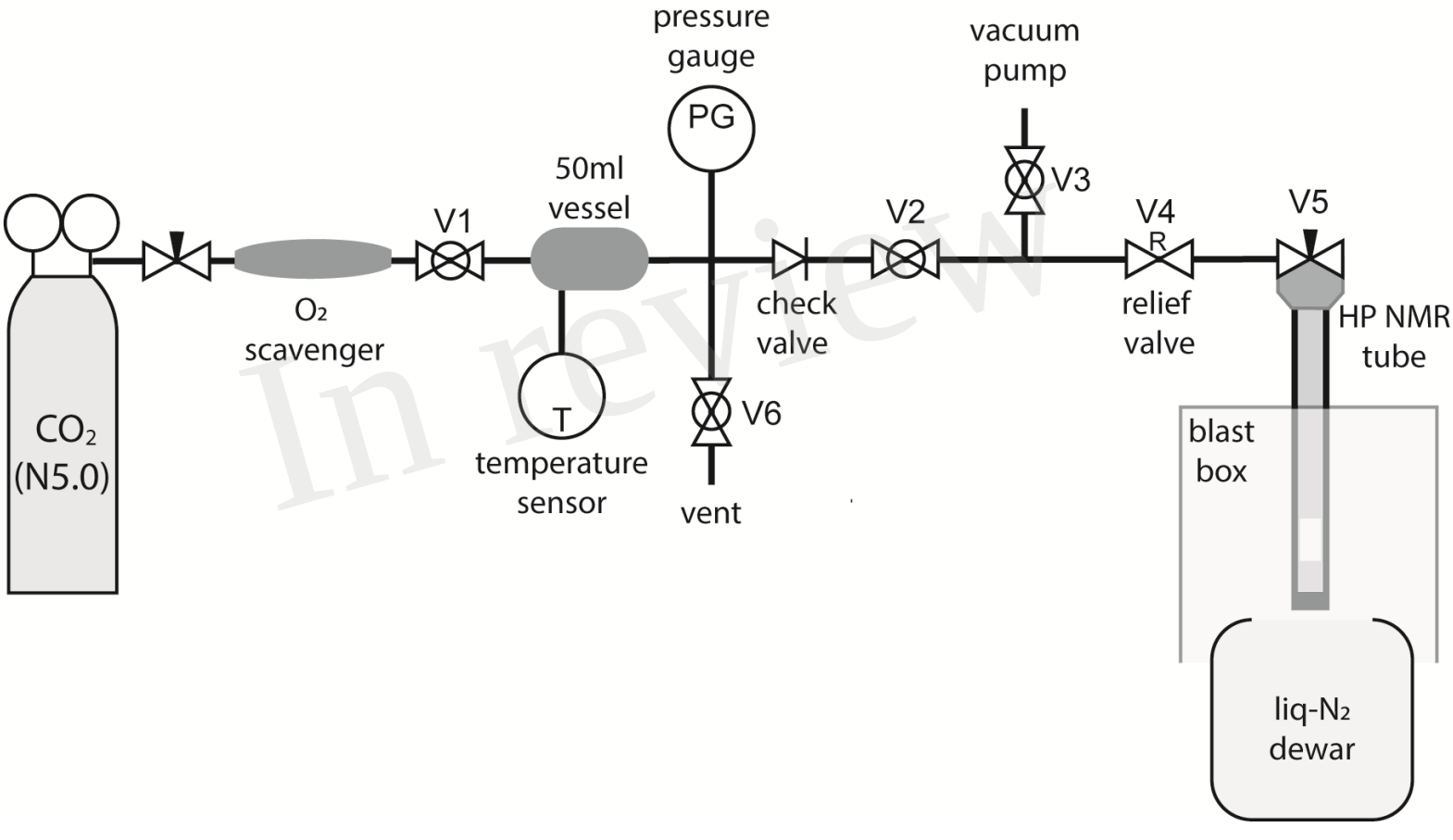

Figure 3.TIF

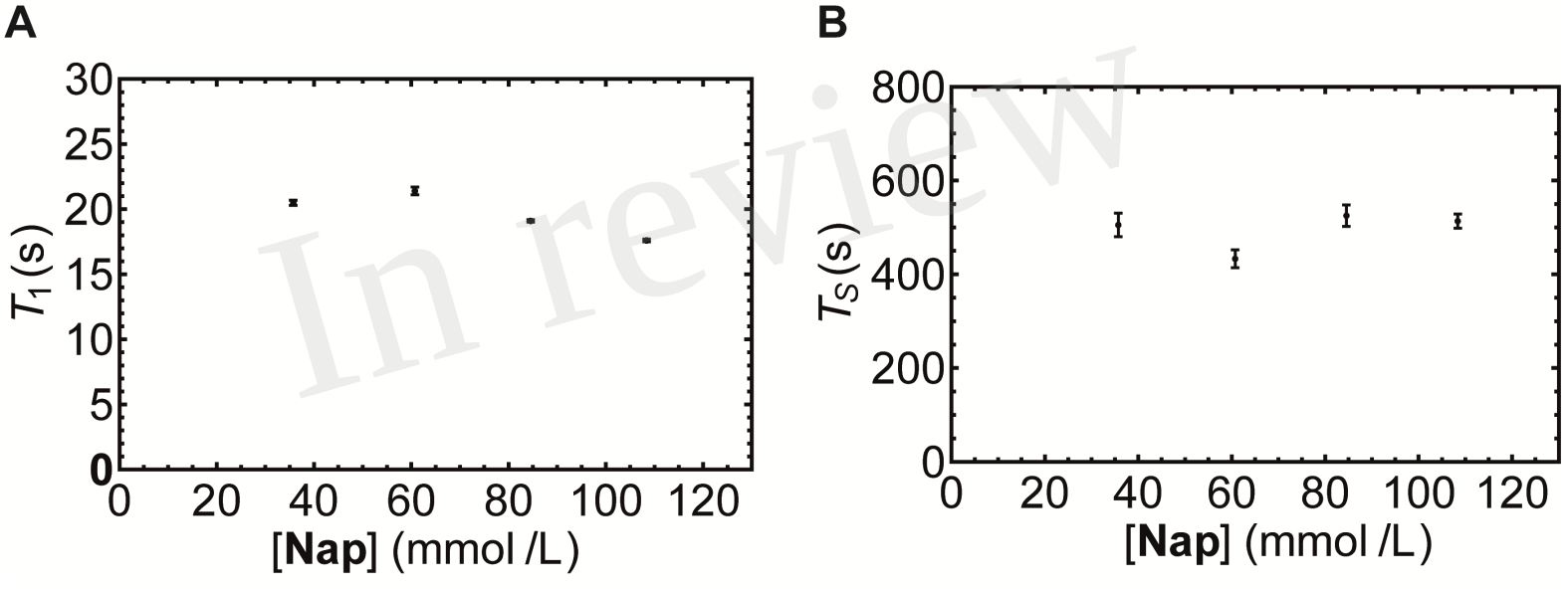

Figure 4.JPEG

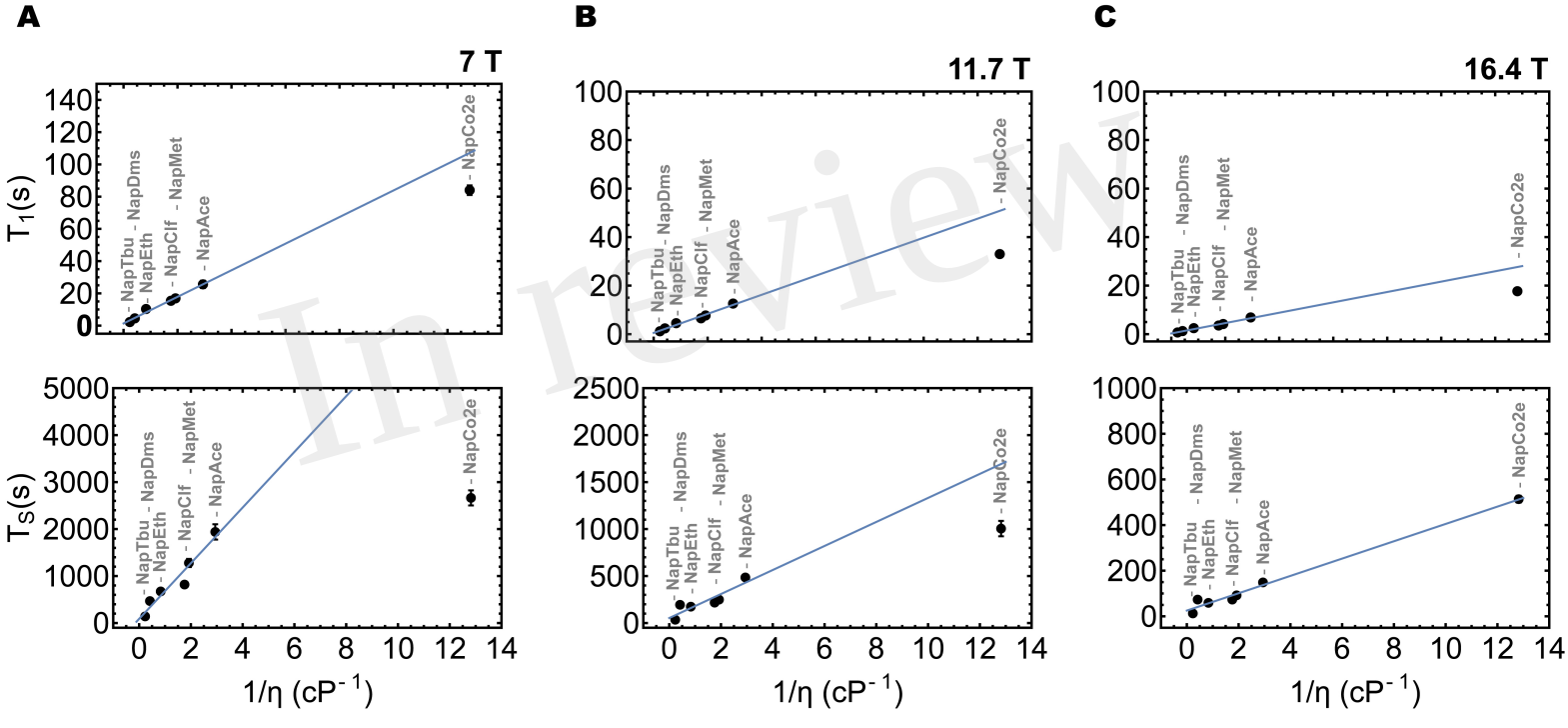

Figure 5.JPEG

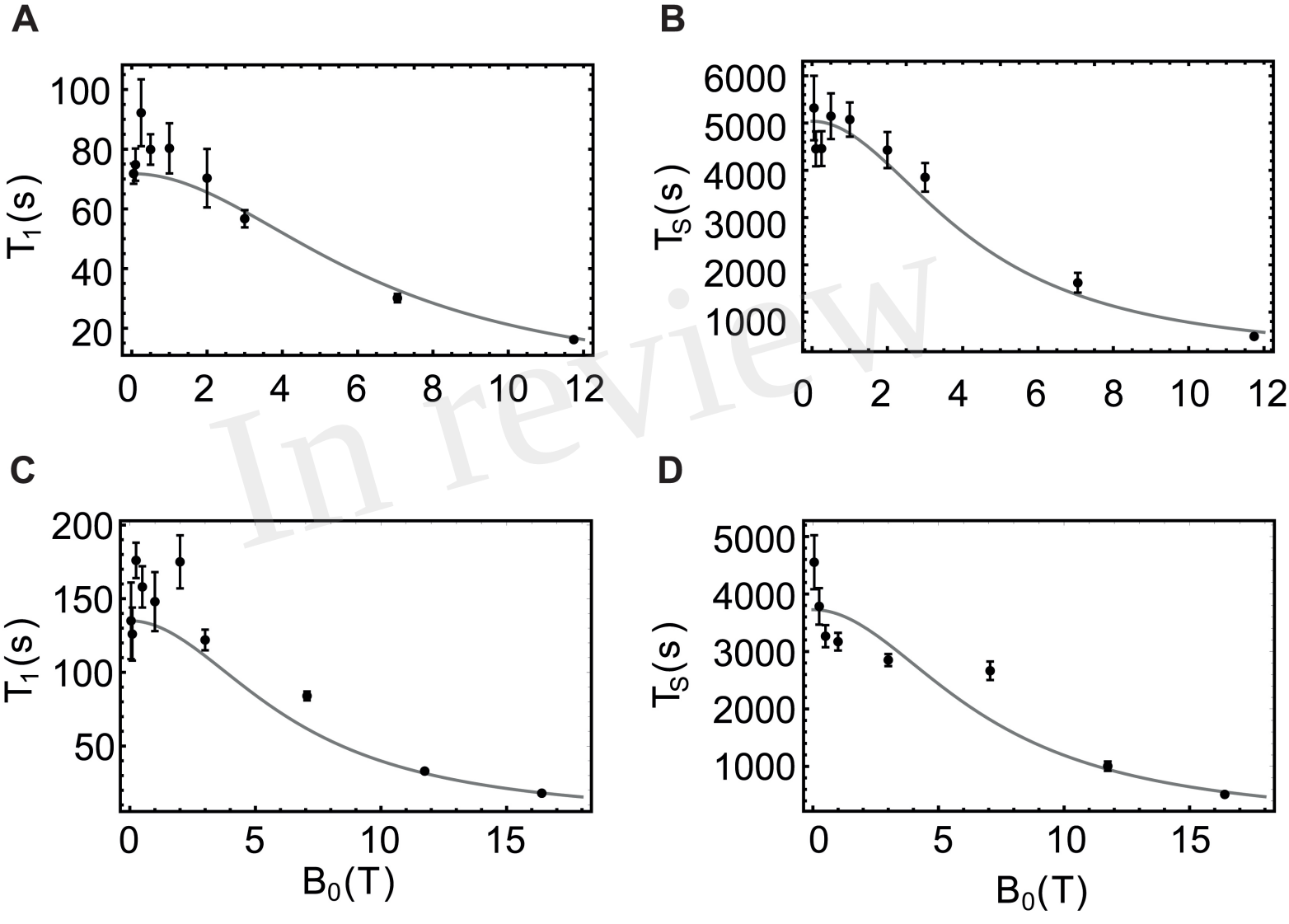

Figure 6.TIF



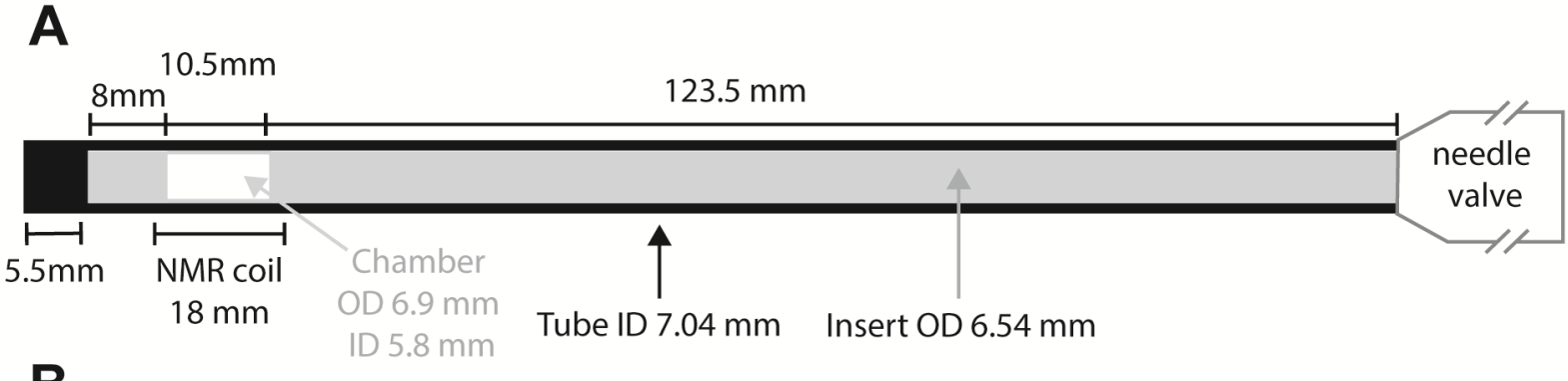


B